

Dynamic responses of an energy harvesting system based on piezoelectric and electromagnetic mechanisms under colored noise

Yong-Ge Yang(杨勇歌), Yun Meng(孟运), Yuan-Hui Zeng(曾远辉), and Ya-Hui Sun(孙亚辉)
Citation: Chin. Phys. B, 2023, 32 (**9**): 090201. DOI: 10.1088/1674-1056/acd621
Journal homepage: http://cpb.iphy.ac.cn; http://iopscience.iop.org/cpb

What follows is a list of articles you may be interested in

Mutation detection and fast identification of switching system based on data-driven method

Zhonghua Zhang(张钟化), Wei Xu(徐伟), and Yi Song(宋怡)
Chin. Phys. B, 2023, 32 (**5**): 050201. DOI: 10.1088/1674-1056/acb9f5

Inverse stochastic resonance in modular neural network with synaptic plasticity

Yong-Tao Yu(于永涛) and Xiao-Li Yang(杨晓丽)
Chin. Phys. B, 2023, 32 (**3**): 030201. DOI: 10.1088/1674-1056/aca602

Inhibitory effect induced by fractional Gaussian noise in neuronal system

Zhi-Kun Li(李智坤) and Dong-Xi Li(李东喜)
Chin. Phys. B, 2023, 32 (**1**): 010203. DOI: 10.1088/1674-1056/ac6332

Sparse identification method of extracting hybrid energy harvesting system from observed data

Ya-Hui Sun(孙亚辉), Yuan-Hui Zeng(曾远辉), and Yong-Ge Yang(杨勇歌)
Chin. Phys. B, 2022, 31 (**12**): 120203. DOI: 10.1088/1674-1056/ac9cbf

Most probable transition paths in eutrophicated lake ecosystem under Gaussian white noise and periodic force

Jinlian Jiang(姜金连), Wei Xu(徐伟), Ping Han(韩平), and Lizhi Niu(牛立志)
Chin. Phys. B, 2022, 31 (**6**): 060203. DOI: 10.1088/1674-1056/ac5616

Dynamic responses of an energy harvesting system based on piezoelectric and electromagnetic mechanisms under colored noise

Yong-Ge Yang(杨勇歌)[1], Yun Meng(孟运)[1], Yuan-Hui Zeng(曾远辉)[1], and Ya-Hui Sun(孙亚辉)[1,2,†]

[1] *School of Mathematics and Statistics, Guangdong University of Technology, Guangzhou* 510520, *China*
[2] *State Key Laboratory for Strength and Vibration of Mechanical Structures, Xi'an Jiaotong University, Xi'an* 710049, *China*

(Received 28 February 2023; revised manuscript received 6 April 2023; accepted manuscript online 17 May 2023)

Because of the increasing demand for electrical energy, vibration energy harvesters (VEHs) that convert vibratory energy into electrical energy are a promising technology. In order to improve the efficiency of harvesting energy from environmental vibration, here we investigate a hybrid VEH. Unlike previous studies, this article analyzes the stochastic responses of the hybrid piezoelectric and electromagnetic energy harvesting system with viscoelastic material under narrow-band (colored) noise. Firstly, a mass-spring-damping system model coupled with piezoelectric and electromagnetic circuits under fundamental acceleration excitation is established, and analytical solutions to the dimensionless equations are derived. Then, the formula of the amplitude-frequency responses in the deterministic case and the first-order and second-order steady-state moments of the amplitude in the stochastic case are obtained by using the multi-scales method. The amplitude-frequency analytical solutions are in good agreement with the numerical solutions obtained by the Monte Carlo method. Furthermore, the stochastic bifurcation diagram is plotted for the first-order steady-state moment of the amplitude with respect to the detuning frequency and viscoelastic parameter. Eventually, the influence of system parameters on mean-square electric voltage, mean-square electric current and mean output power is discussed. Results show that the electromechanical coupling coefficients, random excitation and viscoelastic parameter have a positive effect on the output power of the system.

Keywords: hybrid vibration energy harvesting, narrow-band random excitation, multi-scales method, viscoelastic material, stochastic bifurcation

PACS: 02.50.–r, 05.40.–a, 05.40.Ca **DOI:** 10.1088/1674-1056/acd621

1. Introduction

Sustainable technologies that harvest energy from environmental vibrations for power generation have received considerable attention in recent years.[1–4] Vibration energy harvesters (VEHs) with ability to harvest electrical energy from environmental vibration are a good potential technology to provide continuous electrical energy instead of batteries with limited lifespan.[5] Piezoelectric,[6] electromagnetic,[7] electrostatic[8] and triboelectric[9] transductions are the main technologies for converting environmental vibration into electric energy. To increase the energy conversion efficiency, a hybrid piezoelectric and electromagnetic energy harvesting system (EHS) has been developed. Challa *et al.*[10] developed the hybrid piezoelectric and electromagnetic energy harvesting technology based on a single frequency. Karami *et al.*[11] employed approximation methods to study variations of damping and excitation frequency in a nonlinear hybrid EHS. Li *et al.*[12] studied the mean output power and power spectral density of a hybrid piezoelectric and electromagnetic EHS. Mokem *et al.*[13] proposed a hybrid device combining piezoelectric and electromagnetic transduction under colored noise. Fan *et al.*[14] investigated a hybrid piezoelectric and electromagnetic EHS under low-frequency and multi-directional excitations. Taking advantages of the stochastic averaging technique, Sun *et al.*[15] found that a hybrid vibration EHS can produce a mean output power higher than a piezoelectric or electromagnetic system alone.

Since random factors exist widely in most realistic environments and can affect the dynamical behaviors of a system, it is necessary to investigate the system under random excitation. Rong *et al.*[16] studied the principal resonance of the Duffing oscillator under deterministic and narrow-band random excitation by taking advantage of the multi-scales method and the qualitative analysis method. Liu *et al.*[17] proposed a quasi-conservative stochastic averaging method to investigate the probabilistic responses of a nonlinear VEH driven by exponentially correlated Gaussian colored noise. Jin *et al.*[18] applied the multi-scales method to study a Duffing-type energy harvester with time-delay circuits under narrow-band random excitation. Using the stochastic averaging method, Huang *et al.*[19] studied a strongly nonlinear light damping system with a fractional derivative under Gaussian white noise excitation. Xiao *et al.*[20] found that correlated noise can enhance efficiency of a piezoelectric energy harvester. To improve energy harvesting efficiency, Zhang *et al.*[21] carried out theoretical and numerical studies on an electromechanically coupled VEH under colored noise and periodic excitation. By utilizing the implicit harmonic balance method and the Gaussian

†Corresponding author. E-mail: yahsun@163.com
© 2023 Chinese Physical Society and IOP Publishing Ltd

closure method, Zhu *et al.*[22] discussed the periodic response of a Duffing oscillator under harmonic and random combined excitation. Shi *et al.*[23] studied an asymmetric stochastic resonance system with time-delayed feedback driven by non-Gaussian colored noise. Lin *et al.*[24] invesigated the bursting oscillation and energy harvesting efficiency of a piezoelectric energy harvester in rotational motion under low-frequency excitation. Under Gaussian white noise excitation, Su *et al.*[25] presented a vibration EHS with rigid and elastic impacts. Jiang *et al.*[26] designed an electromechanical broadband energy harvester with one-to-one internal resonance.

Viscoelastic materials, in contrast to conventional elastic materials, can not only store elastic potential energy but also dissipate energy.[27] Furthermore, viscoelastic materials with viscoelastic properties like stress relaxation and creep are more suitable for describing practical problems, so they are widely used in physics, mathematics, engineering, and other fields.[28–31] Xu *et al.*[32] investigated a narrow-band noise system with fractional damping and viscoelastic term. Guo *et al.*[33] discussed the stochastic responses of an EHS with viscoelastic material excited by Gaussian white noise. Wu *et al.*[34] analyzed the initial boundary value problem for the viscoelastic equation in a bounded region. By utilizing the harmonic balance method and the stochastic averaging method, Xu *et al.*[35] obtained the responses of a viscoelastic system under the combination of deterministic harmonic and random excitation. Floris *et al.*[36] studied the stability of hinged-hinged viscoelastic column under non-zero mean stochastic axial force. Denoël *et al.*[37] carried out the multiple timescale spectral analysis of a single-degree-of-freedom viscoelastic system with a fractional derivative.

Recently, there are several papers[38–41] focused on vibration EHSs with viscoelastic materials. In Refs. [38,39] the authors adopted the stochastic averaging method to investigate EHSs. In Refs. [40,41] the authors studied a single type of piezoelectric EHSs by applying the multi-scales method. The vital difference between our study and the above-mentioned studies is that we consider a hybrid vibration EHS subjected to narrow-band noise excitation by employing the multi-scales method.

The remainder of this paper is organized as follows. In Section 2, we present the basic mathematical model of the hybrid piezoelectric and electromagnetic EHS with viscoelastic material under narrow-band noise excitation. In Section 3, the approximate solutions for the hybrid vibration EHS are obtained by employing the multi-scales method. The analytical results are verified by numerical simulation results obtained with the Monte Carlo method. Moreover, the stochastic responses and the stochastic bifurcation phenomena of the system are further explored. In Section 4, the influence of the system parameters on mean-square electric voltage, mean-square electric current and mean output power is discussed. Finally. the conclusions are given in Section 5.

2. Mathematical model

So far, several different nonlinear vibrational energy harvesters with high conversion efficiency have been designed.[42–44] Taking the hybrid piezoelectric and electromagnetic energy harvester as an example, it can be modeled as a mass-spring-damping system coupled with piezoelectric and electromagnetic circuits under fundamental acceleration excitation.[45–47] The simplified structural schematic and the simplified representation of the piezoelectric and electromagnetic circuits are shown in Figs. 1(a)–1(c), respectively.

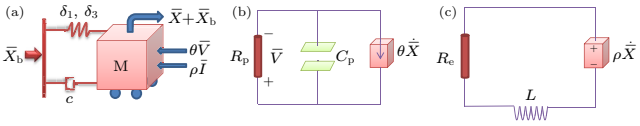


Fig. 1. (a) A simplified structural schematic of the hybrid VEH with (b) piezoelectric and (c) electromagnetic circuits.

In order to illustrate the mechanical property of viscoelastic material in damping structure, a hybrid VEH with viscoelastic material[48,49] is presented in Fig. 2.

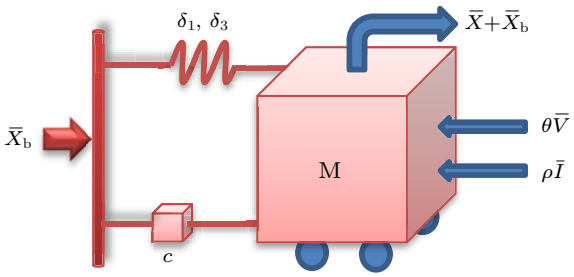


Fig. 2. A simplified representation of the hybrid VEH with viscoelastic material.

The governing equations of the hybrid VEH can be written in the following general form:

$$\begin{aligned}
&M\ddot{\overline{X}}+cH(\beta,\overline{X},t)+\delta_1\overline{X}+\delta_3\overline{X}^3+\theta\overline{V}+\rho\overline{I}=-M\ddot{\overline{X}}_b,\\
&C_p\dot{\overline{V}}+\frac{\overline{V}}{R_p}=\theta\dot{\overline{X}},\\
&L\dot{I}+(R_c+R_e)\overline{I}=\rho\dot{\overline{X}},
\end{aligned}\tag{1}$$

where the symbols for the hybrid vibration EHS are listed in Table 1.

We introduce the dimensionless transformations as follows:

$$\begin{aligned}
&x=\overline{X},\ x_b=\overline{X}_b,\ v=\frac{C_p}{\theta}\overline{V},\ i=\frac{L}{\rho}\overline{I},\ \tau=\omega t,\ \omega=\sqrt{\frac{\delta_1}{M}},\\
&\alpha_1=\frac{c}{\delta_1},\ \alpha_3=\frac{\delta_3}{\delta_1},\ k_1=\frac{\theta^2}{\delta_1 C_p},\ k_2=\frac{\rho^2}{\delta_1 L},\\
&\lambda_1=\frac{1}{R_pC_p\omega},\ \lambda_2=\frac{R_c+R_e}{L\omega}.
\end{aligned}\tag{2}$$

Then the dimensionless form of Eq. (1) is given as

$$\begin{aligned}&\ddot{x}+\alpha_1 H(\beta\omega,x,\tau)+x+\alpha_3 x^3+k_1 v+k_2 i=-\ddot{x}_{\rm b},\\&\dot{v}+\lambda_1 v=\dot{x},\\&\dot{i}+\lambda_2 i=\dot{x}.\end{aligned}\tag{3}$$

The definitions of symbols are listed in Table 2.

Table 1. Symbols and definitions.

Symbol	Definitions
$\overline{X}$	Relative displacement
c	Viscoelastic coefficient
δ_1	Linear stiffness coefficient
δ_3	Nonlinear stiffness coefficient
θ	Piezoelectric force-voltage factor
ρ	Electromagnetic force-current factor
$\overline{I}$	Piezoelectric current
$C_{\rm p}$	Piezoelectric capacitance
$R_{\rm e}$	Load resistance
$R_{\rm p}$	Load resistance
L	Coil inductance
$R_{\rm c}$	Coil resistance

Table 2. Symbols and definitions.

Symbol	Definitions
k_1	Electromechanical coupling coefficient
k_2	Electromechanical coupling coefficient
λ_1	Inverse of the product of the resistor and capacitor
λ_2	Ratio of resistance and inductance

Here, $-\ddot{x}_{\rm b}$ is equivalent to noise $\xi(\tau)$, which stands for a narrow-band random process and can be written as[50]

$$\xi(\tau)=\hat{F}\cos\left[\frac{\Omega\tau}{\omega}+\gamma W\left(\frac{\tau}{\omega}\right)\right],\tag{4}$$

where γ is the intensity of the random excitation, $W(\tau)$ is a standard Wiener process, ω denotes the excitation frequency, and $\hat{F}$ is the deterministic amplitude.

The viscoelastic term $H(\beta\omega,x,\tau)$ is derived as[32]

$$\begin{aligned}H(\beta,x,t)&=\int_0^t\frac{1}{\beta}\exp\Big(-\frac{t-s}{\beta}\Big)x(s)\mathrm{d}s\\&\overset{\tau=\omega t}{=}\int_0^\tau\frac{1}{\beta}\exp\Big[\Big(-\frac{1}{\beta}\Big(\frac{\tau}{\omega}-\frac{\eta_1}{\omega}\Big)\Big]x(\eta_1)\mathrm{d}\frac{\eta_1}{\omega}\\&=\int_0^\tau\frac{1}{\beta\omega}\exp\Big(-\frac{\tau-\eta_1}{\beta\omega}\Big)x(\eta_1)\mathrm{d}\eta_1\\&=H(\beta\omega,x,\tau).\end{aligned}\tag{5}$$

According to Ref. [51], the power spectrum density $S_\xi(\omega)$ of $\xi(\tau)$ can be expressed as

$$S_\xi(\omega)=\frac{1}{2}\frac{\gamma^2(\Omega^2+\omega^2+\gamma^4/4)}{(\Omega^2-\omega^2+\gamma^4/4)^2+\omega^2\gamma^4},\tag{6}$$

where the random process $\xi(\tau)$ can be considered as a narrow band process when γ is small.

3. Response analysis

For convenience, we introduce the following transformations:

$$\alpha_1=\varepsilon\beta_1,\ \alpha_3=\varepsilon\mu,\ k_1=\varepsilon q,\ k_2=\varepsilon g,\ \hat{F}=\varepsilon F.\tag{7}$$

Then, substituting Eqs. (4) and (7) into Eq. (3), we have

$$\begin{aligned}&\ddot{x}+\varepsilon\beta_1 H(\beta\omega,x,\tau)+x+\varepsilon\mu x^3+\varepsilon q v+\varepsilon g i\\&=\varepsilon F\cos\left[\frac{\Omega\tau}{\omega}+\gamma W\left(\frac{\tau}{\omega}\right)\right],\\&\dot{v}+\lambda_1 v=\dot{x},\quad \dot{i}+\lambda_2 i=\dot{x},\end{aligned}\tag{8}$$

in which the over-dot prime represents the derivative with respect to the time variable τ. In this paper, the multiple scales method[16,18,52] is employed to investigate the responses of the system (3). Taking advantage of the modified multi-scales method, we introduce fast and slow time scales as follows:

$$T_0=\tau,\quad T_1=\varepsilon\tau.\tag{9}$$

Introducing

$$D_0=\partial/\partial T_0,\quad D_1=\partial/\partial T_1,\tag{10}$$

the ordinary time derivatives can be transformed into partial derivatives as

$$\frac{\mathrm{d}}{\mathrm{d}\tau}=D_0+\varepsilon D_1+\cdots,\quad \frac{\mathrm{d}^2}{\mathrm{d}\tau^2}=D_0^2+2\varepsilon D_0D_1+\cdots.\tag{11}$$

The approximate solutions of Eq. (8) are given as follows:

$$x=x_0(T_0,T_1)+\varepsilon x_1(T_0,T_1)+\cdots,\tag{12a}$$

$$v=v_0(T_0,T_1)+\varepsilon v_1(T_0,T_1)+\cdots,\tag{12b}$$

$$i=i_0(T_0,T_1)+\varepsilon i_1(T_0,T_1)+\cdots.\tag{12c}$$

Substituting Eqs. (10)–(12) into Eq. (8), and equating the coefficients of ε^0 and ε^1 to zeros, the formulas at the first order can be written as

$$D_0^2x_0+x_0=0,\tag{13a}$$

$$D_0v_0+\lambda_1v_0=D_0x_0,\tag{13b}$$

$$D_0i_0+\lambda_2i_0=D_0x_0.\tag{13c}$$

The formulas in the second order can be given as

$$\begin{aligned}D_0^2x_1+x_1=&-2D_0D_1x_0-\beta_1H(\beta\omega,x,\tau)\\&-\mu x_0^3-qv_0-gi_0\\&+F\cos\left[\frac{\Omega\tau}{\omega}+\frac{\gamma}{\sqrt{\omega}}W(\tau)\right],\end{aligned}\tag{14a}$$

$$D_0v_1+\lambda_1v_1=-D_1v_0+D_0x_1+D_1x_0,\tag{14b}$$

$$D_0i_1+\lambda_2i_1=-D_1i_0+D_0x_1+D_1x_0.\tag{14c}$$

In Eq. (14a), according to the property of the standard wiener process, we obtain

$$\gamma W(t)=\gamma W\left(\frac{\tau}{\omega}\right)=\frac{\gamma}{\sqrt{\omega}}W(\tau).\tag{15}$$

The general solution of Eq. (13) can be written as

$$x_0(T_0,T_1)=A(T_1)\mathrm{e}^{\mathrm{i}T_0}+\overline{A}(T_1)\mathrm{e}^{-\mathrm{i}T_0}, \tag{16a}$$

$$v_0(T_0,T_1)=B(T_1)\mathrm{e}^{\mathrm{i}T_0}+\overline{B}(T_1)\mathrm{e}^{-\mathrm{i}T_0}, \tag{16b}$$

$$i_0(T_0,T_1)=C(T_1)\mathrm{e}^{\mathrm{i}T_0}+\overline{C}(T_1)\mathrm{e}^{-\mathrm{i}T_0}, \tag{16c}$$

where $\overline{A}$ is the complex conjugate of A, $\overline{B}$ is the complex conjugate of B, $\overline{C}$ is the complex conjugate of C.

Substituting Eqs. (16a) and (16b) into Eq. (13b), B is derived as

$$B(T_1)=\frac{1+\lambda_1\mathrm{i}}{1+\lambda_1^2}A(T_1), \tag{17}$$

where $A(T_1)$ is the slowly varying amplitude of the solution.

Similarly, substituting Eqs. (16a) and (16c) into Eq. (13c), we can obtain the relationship between C and A as follows:

$$C(T_1)=\frac{1+\lambda_2\mathrm{i}}{1+\lambda_2^2}A(T_1). \tag{18}$$

The viscoelastic term $H(\beta\omega,x_0,T_0)$ is written as

$$\begin{aligned}H(\beta\omega,x_0,T_0)&=\int_0^{T_0}\frac{1}{\beta\omega}\exp^{-\frac{T_0-\eta}{\beta\omega}}x_0(s)\mathrm{d}s\\&=\frac{A_0}{\beta\omega}\exp^{-\frac{T_0}{\beta\omega}}\int_0^{T_0}\exp^{(\frac{1}{\beta\omega}+\mathrm{i})s}\mathrm{d}s+\mathrm{c.c.}\\&=\frac{1-\mathrm{i}\beta\omega}{1+(\beta\omega)^2}x_0-\frac{1-\mathrm{i}\beta\omega}{1+(\beta\omega)^2}A\exp^{-\frac{T_0}{\beta\omega}}+\mathrm{c.c.},\end{aligned} \tag{19}$$

where c.c. denotes the conjugate term.

Substituting Eqs. (16)–(19) into Eq. (14a) and eliminating the secular terms, we obtain

$$\begin{aligned}&-2\mathrm{i}D_1A\mathrm{e}^{\mathrm{i}T_0}-\beta_1A\frac{1-\beta\omega\mathrm{i}}{1+(\beta\omega)^2}\mathrm{e}^{\mathrm{i}T_0}-\mu(3A^2\overline{A}\mathrm{e}^{\mathrm{i}T_0})\\&-q\Big(\frac{1+\mathrm{i}\lambda_1}{1+\lambda_1^2}A\mathrm{e}^{\mathrm{i}T_0}\Big)-g\Big(\frac{1+\mathrm{i}\lambda_2}{1+\lambda_2^2}A\mathrm{e}^{\mathrm{i}T_0}\Big)\\&+\frac{1}{2}F\mathrm{e}^{\mathrm{i}\left(\frac{\Omega\tau}{\omega}+\frac{\gamma}{\sqrt{\omega}}W(\tau)\right)}=0.\end{aligned} \tag{20}$$

Letting

$$\begin{aligned}A(T_1)&=\frac{1}{2}a(T_1)\mathrm{e}^{\mathrm{i}\Phi(T_1)},\\\Phi&=\sigma T_1-\eta+\overline{\gamma}W(T_1),\end{aligned} \tag{21}$$

where

$$\frac{\gamma}{\sqrt{\omega}}W(\tau)=\frac{\gamma}{\sqrt{\omega}}W\Big(\frac{T_1}{\varepsilon}\Big)=\frac{\gamma}{\sqrt{\varepsilon\omega}}W(T_1)=\overline{\gamma}W(T_1).$$

The excitation frequency Ω close to the system frequency ω is determined in order to study the primary resonance, that is,

$$\Omega=\omega(1+\varepsilon\sigma). \tag{22}$$

Substituting Eqs. (21) and (22) into Eq. (20), we arrive at

$$\begin{aligned}&-\mathrm{i}D_1a+aD_1\Phi(T_1)-\frac{1}{2}a\beta_1\frac{1-\mathrm{i}\beta\omega}{1+(\beta\omega)^2}-\frac{3}{8}\mu a^3\\&-\frac{1}{2}aq\frac{1+\mathrm{i}\lambda_1}{1+\lambda_1^2}-\frac{1}{2}ag\frac{1+\mathrm{i}\lambda_2}{1+\lambda_2^2}+\frac{1}{2}F\mathrm{e}^{\mathrm{i}\eta}=0.\end{aligned} \tag{23}$$

The differential equations for the amplitude a and phase η with regard to the slow timescale T_1 are obtained by splitting Eq. (23) into the real and imaginary portions

$$D_1a=\frac{1}{2}\frac{a\beta_1\beta\omega}{1+(\beta\omega)^2}-\frac{1}{2}\frac{aq\lambda_1}{1+\lambda_1^2}-\frac{1}{2}\frac{ag\lambda_2}{1+\lambda_2^2}+\frac{1}{2}F\sin\eta, \tag{24a}$$

$$\begin{aligned}aD_1\eta=&a\sigma-\frac{1}{2}\frac{a\beta_1}{1+(\beta\omega)^2}-\frac{3}{8}\mu a^3-\frac{1}{2}\frac{aq}{1+\lambda_1^2}\\&-\frac{1}{2}\frac{ag}{1+\lambda_2^2}+a\overline{\gamma}D_1W(T_1)+\frac{1}{2}F\cos\eta.\end{aligned} \tag{24b}$$

Therefore, by solving Eq. (24), combining Eqs. (16a)–(18), (21)–(22) and (24), the first-order approximate solutions of the hybrid vibration EHS (3) can be written as

$$x=a(\varepsilon\tau)\cdot\cos\Big(\frac{\Omega\tau}{\omega}-\eta(\varepsilon\tau)\Big)+O(\varepsilon), \tag{25a}$$

$$v=\frac{a(\varepsilon\tau)}{\sqrt{1+\lambda_1^2}}\cos\Big(\frac{\Omega\tau}{\omega}-\eta(\varepsilon\tau)+\arctan\lambda_1\Big)+O(\varepsilon), \tag{25b}$$

$$i=\frac{a(\varepsilon\tau)}{\sqrt{1+\lambda_2^2}}\cos\Big(\frac{\Omega\tau}{\omega}-\eta(\varepsilon\tau)+\arctan\lambda_2\Big)+O(\varepsilon). \tag{25c}$$

In particular, we focus on the fit between the theoretical and the numerical results for the amplitude-frequency responses, which validates the analytical approach described above.

When $\gamma=0$, the deterministic steady-state solutions $a=a_0$ and $\eta=\eta_0$ of Eq. (24) satisfy $D_1a=0$ and $D_1\eta=0$, then Eq. (24) becomes

$$\frac{1}{2}\frac{a_0\beta_1\beta\omega}{1+(\beta\omega)^2}-\frac{1}{2}\frac{a_0q\lambda_1}{1+\lambda_1^2}-\frac{1}{2}\frac{a_0g\lambda_2}{1+\lambda_2^2}+\frac{1}{2}F\sin\eta_0=0, \tag{26a}$$

$$\begin{aligned}&a_0\sigma-\frac{1}{2}\frac{a_0\beta_1}{1+(\beta\omega)^2}-\frac{3}{8}\mu a_0^3-\frac{1}{2}\frac{a_0q}{1+\lambda_1^2}\\&-\frac{1}{2}\frac{a_0g}{1+\lambda_2^2}+\frac{1}{2}F\cos\eta_0=0.\end{aligned} \tag{26b}$$

After eliminating η_0 from Eq. (26), the equation of amplitude-frequency responses is obtained as follows:

$$\begin{aligned}\sigma=&\frac{1}{2}\frac{\beta_1}{1+(\beta\omega)^2}+\frac{1}{2}\frac{q}{1+\lambda_1^2}+\frac{1}{2}\frac{g}{1+\lambda_2^2}\\&+\frac{3}{8}\mu a_0^2\mp\sqrt{\frac{F^2}{4a_0^2}-(G_1)^2},\end{aligned} \tag{27}$$

with

$$G_1=\frac{1}{2}\frac{q\lambda_1}{1+\lambda_1^2}+\frac{1}{2}\frac{g\lambda_2}{1+\lambda_2^2}-\frac{1}{2}\frac{\beta_1\beta\omega}{1+(\beta\omega)^2}.$$

When $\gamma\neq0$, in order to determine the stability of the non-trivial steady state solutions, we let

$$a=a_0+a_1,\quad \eta=\eta_0+\eta_1, \tag{28}$$

where a_1 and η_1 are the perturbation terms on the deterministic situations.

Substituting Eqs. (26) and (28) into Eq. (24) and neglecting the nonlinear terms, the Itôstochastic differential equations are obtained as follows:

$$\mathrm{d}a_1 = (S_{11}a_1 + S_{12}\eta_1)\mathrm{d}T_1, \tag{29a}$$

$$\mathrm{d}\eta_1 = (S_{21}a_1 + S_{22}\eta_1)\mathrm{d}T_1 + \overline{\gamma}\mathrm{d}W(T_1), \tag{29b}$$

where

$$\begin{aligned}
S_{11} &= \frac{1}{2}\frac{\beta_1\beta\omega}{1+(\beta\omega)^2} - \frac{1}{2}\frac{q\lambda_1}{1+\lambda_1^2} - \frac{1}{2}\frac{g\lambda_2}{1+\lambda_2^2},\\
S_{12} &= \frac{F}{2}\cos\eta_0 = \frac{1}{2}\frac{a_0\beta_1}{1+(\beta\omega)^2} - a_0\sigma + \frac{3}{8}\mu a_0^3 + \frac{1}{2}\frac{a_0 q}{1+\lambda_1^2}\\
&\quad + \frac{1}{2}\frac{a_0 g}{1+\lambda_2^2},\\
S_{21} &= \frac{\sigma}{a_0} - \frac{1}{2}\frac{\beta_1}{a_0(1+(\beta\omega)^2)} - \frac{9}{8}\mu a_0 - \frac{1}{2}\frac{q}{a_0(1+\lambda_1^2)}\\
&\quad - \frac{1}{2}\frac{g}{a_0(1+\lambda_2^2)},\\
S_{22} &= -\frac{F}{2a_0}\sin\eta_0 = \frac{1}{2}\frac{\beta_1\beta\omega}{1+(\beta\omega)^2} - \frac{1}{2}\frac{q\lambda_1}{1+\lambda_1^2} - \frac{1}{2}\frac{g\lambda_2}{1+\lambda_2^2}.
\end{aligned}$$

Under the steady-state situation, it is known that

$$\frac{\mathrm{d}E(a_1)}{\mathrm{d}T_1} = \frac{\mathrm{d}E(\eta_1)}{\mathrm{d}T_1} = \frac{\mathrm{d}E(a_1^2)}{\mathrm{d}T_1} = \frac{\mathrm{d}E(\eta_1^2)}{\mathrm{d}T_1} = \frac{\mathrm{d}E(a_1\eta_1)}{\mathrm{d}T_1} = 0, \tag{30}$$

where $E(\cdot)$ denotes the mathematical expectation.

Combining Eqs. (29) and (30), one can obtain

$$\begin{aligned}
&2S_{11}E(a_1^2) + 2S_{12}E(a_1\eta_1) = 0,\\
&S_{21}E(a_1^2) + (S_{22}+S_{11})E(a_1\eta_1) + S_{12}E(\eta_1^2) = 0,\\
&2S_{21}E(a_1\eta_1) + 2S_{22}E(\eta_1^2) + \overline{\gamma}^2 = 0.
\end{aligned} \tag{31}$$

Solving Eq. (31), we can obtain the first-order and second-order steady-state moments (FSSMs) of a_1 and η_1 as

$$\begin{aligned}
&E(a_1) = 0, \quad E(\eta_1) = 0,\\
&E(a_1^2) = \frac{-2S_{12}^2\overline{\gamma}^2}{Q_1}, \quad E(\eta_1^2) = \frac{Q_2}{2S_{12}S_{22}},
\end{aligned} \tag{32}$$

where

$$\begin{aligned}
Q_1 &= 4(S_{11}S_{22}^2 + S_{11}^2S_{22} - S_{12}S_{21}S_{22} - S_{11}S_{12}S_{21}),\\
Q_2 &= 2S_{11}S_{21}Ea_1^2 - S_{12}\overline{\gamma}^2.
\end{aligned}$$

Therefore, the FSSMs of the steady-state solutions to Eq. (24) are given as

$$\begin{aligned}
&E(a) = a_0, \quad E(\eta) = \eta_0,\\
&E(a^2) = a_0^2 + \frac{-2S_{12}^2\overline{\gamma}^2}{Q_1}, \quad E(\eta^2) = \eta_0^2 + \frac{Q_2}{2S_{12}S_{22}}.
\end{aligned} \tag{33}$$

In the steady-state case, the voltage and current of the response are obtained by Eqs. (25b) and (25c), respectively,

$$v = \frac{a}{\sqrt{1+\lambda_1^2}}, \tag{34a}$$

$$i = \frac{a}{\sqrt{1+\lambda_2^2}}. \tag{34b}$$

Taking the expectation on both sides of Eq. (34), the FSSMs of the voltage and current amplitude are

$$E(v) = \frac{E(a)}{\sqrt{1+\lambda_1^2}}, \quad E(v^2) = \frac{E(a^2)}{1+\lambda_1^2}, \tag{35a}$$

$$E(i) = \frac{E(a)}{\sqrt{1+\lambda_2^2}}, \quad E(i^2) = \frac{E(a^2)}{1+\lambda_2^2}. \tag{35b}$$

Since the mean output power of the hybrid vibration EHS is the sum of the mean output power of the electromagnetic and piezoelectric circuits, the mean output power can be expressed as

$$\begin{aligned}
E(P) &= E(P_v) + E(P_i) = k_1\lambda_1 E(v^2) + k_2\lambda_2 E(i^2)\\
&= \left(\frac{k_1\lambda_1}{\lambda_1^2+1} + \frac{k_2\lambda_2}{\lambda_2^2+1}\right)\left(a_0^2 + \frac{-2S_{12}^2\overline{\gamma}^2}{Q_1}\right).
\end{aligned} \tag{36}$$

The numerical solution to Eq. (8) is calculated by the fourth-order Runge–Kutta algorithm. In the present numerical computation, we take parameters as $\varepsilon = 0.1$, $\beta = 3$, $\omega = 1.5$, $F = 1.6$, $\beta_1 = 1$, $\mu = 2$, $q = 1.2$, $g = 1$, $\lambda_1 = 3$, $\lambda_2 = 2$.

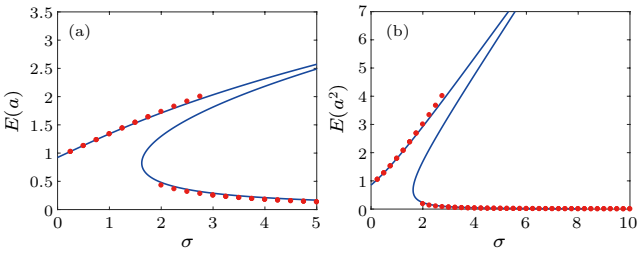


Fig. 3. The FSSMs $E(a)$ (a) and $E(a^2)$ (b) of amplitude-frequency response ($\gamma = 0.01$, $\beta = 3$). Red dots denote the numerical results, blue lines stand for the approximate analytical results.

The numerical results in Fig. 3 are presented to verify the theoretical results obtained from Eqs. (32) and (33). The FSSMs for random excitation $\gamma = 0.01$ are displayed in Fig. 3, and it can be seen that the numerical and approximate analytical results are in good agreement with each other.

In the following numerical simulation, the time history and phase trajectory of system (8), beginning from initial values $x(\tau) = 0.7$, $\dot{x}(\tau) = 0.3$, $v(\tau) = 0.01$, $i(\tau) = 0.01$, with different noise intensities γ and detuning frequencies σ, are shown in Fig. 4. When the intensity of random excitation γ increases, the output responses of displacement $x(\tau)$ and velocity $\dot{x}(\tau)$ change, and the phase trajectory transforms from a limit cycle into a diffused limit cycle in Fig. 4. At different

detuning frequencies σ, the responses of displacement $x(\tau)$, velocity $\dot{x}(\tau)$, voltage $v(\tau)$, and current $i(\tau)$ are depicted in Fig. 5, where the responses of the system increase slowly and then sharply decrease in $\sigma \in (2.5, 3.0)$. Therefore, when the detuning frequency σ gradually increases, the jump can occur.

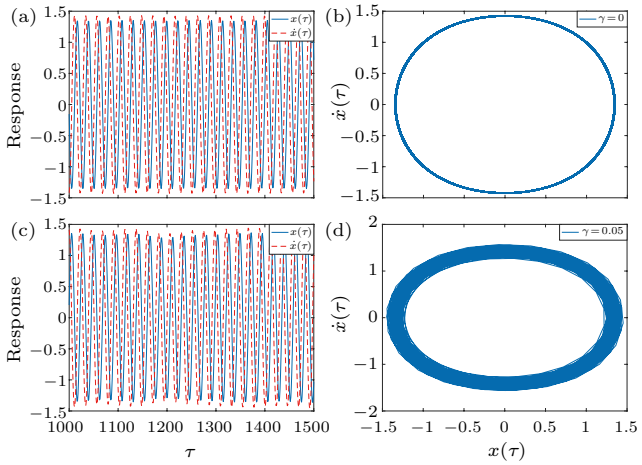


Fig. 4. Time history and phase portraits for the deterministic system ($\sigma = 1$): [(a), (b)] $\gamma = 0$, [(c), (d)] $\gamma = 0.05$.

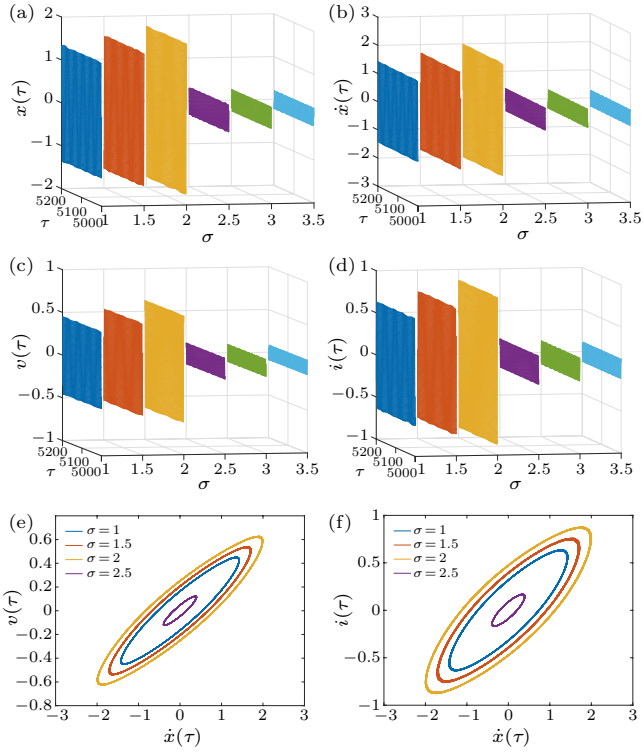


Fig. 5. The stochastic response and phase plot under different frequencies σ for (a)–(f) $\gamma = 0.01$.

Due to the existence of multiple coexisting attractors, the random components superimposed on the harmonic excitation will lead to different dynamic behaviors with different parameter values, which is called the stochastic bifurcation.[40,53] Figure 6 shows the bifurcation diagram about the steady-state moment $E(a)$ under σ and β. The number of system solutions $E(a)$ is analyzed by employing the detuning frequency σ and viscoelastic parameter β as bifurcation parameters, and the corresponding bifurcation diagram is shown in Fig. 7. The bifurcation diagram is divided into parts I and II, representing one solution and three solutions of $E(a)$, respectively. For a fixed β, the number of the system solutions $E(a)$ changes from 1 to 3 and then from 3 to 1 with increasing the parameter σ, which verifies the stochastic jump phenomenon of the hybrid EHS in Fig. 5.

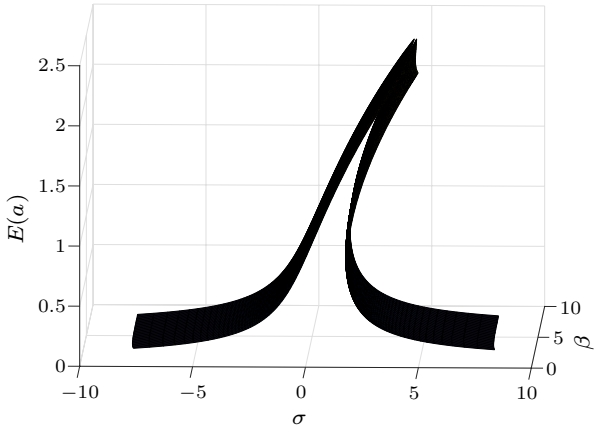


Fig. 6. Bifurcation diagram of $E(a)$ solutions versus σ and β.

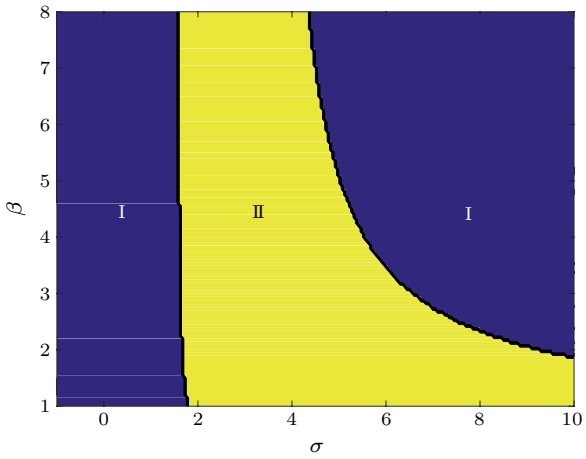


Fig. 7. Bifurcation diagram of the number of $E(a)$ solutions versus σ and β.

4. Efficiency analysis of energy harvesting

The mean-square electric voltage $E(v^2)$, mean-square electric current $E(i^2)$, second-order steady-state moment $E(a^2)$, and mean output power $E(P)$ are indicators that can measure the efficiency of energy harvesting. In this section, we mainly pay attention to the changes of $E(v^2)$, $E(i^2)$, and $E(P)$ under different parameters.

Within a certain noise intensity γ, the effects of the electromechanical coupling coefficient q, the inverse of the product of the resistor and capacitor λ_1 and the viscoelastic parameter β on $E(v^2)$ are depicted in Figs. 8(a), 8(b), and 8(e), and the effects of the electromechanical coupling coefficient g, the ratio of resistance and inductance λ_2 and the viscoelastic parameter β on $E(i^2)$ are shown in Figs. 8(c), 8(d), and 8(f), re-

spectively. On the one hand, $E(v^2)$ decreases with increasing the parameter q or λ_1 in Figs. 8(a) and 8(b), and similarly $E(i^2)$ decreases with increasing the parameter g or λ_2 in Figs. 8(c) and 8(d). Figures 8(e) and 8(f) show that $E(v^2)$ and $E(i^2)$ increase with the increase of the viscoelastic parameter β. On the other hand, $E(v^2)$ and $E(i^2)$ increase with increasing γ in Figs. 8(a)–8(f).

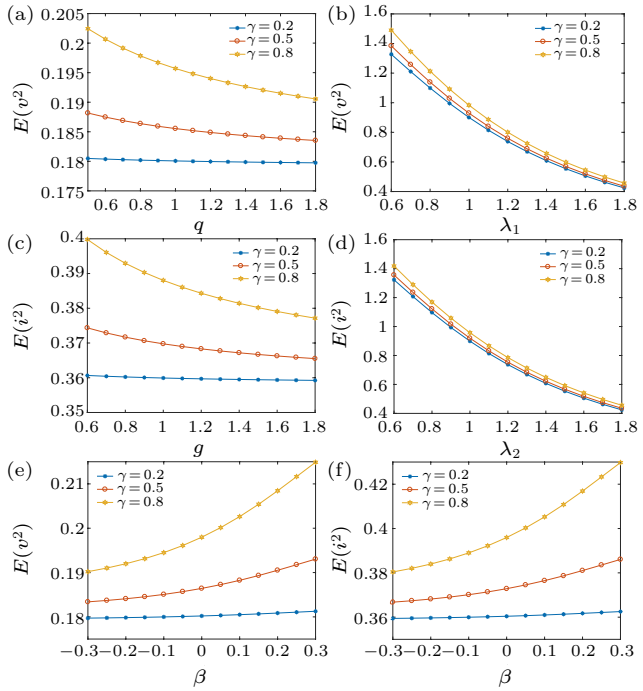


Fig. 8. $E(v^2)$ and $E(i^2)$ decreasing with increasing (a) q, (b) λ_1, (c) g, and (d) λ_2 for different γ ($\sigma = 1$), while increasing with [(e), (f)] increasing β.

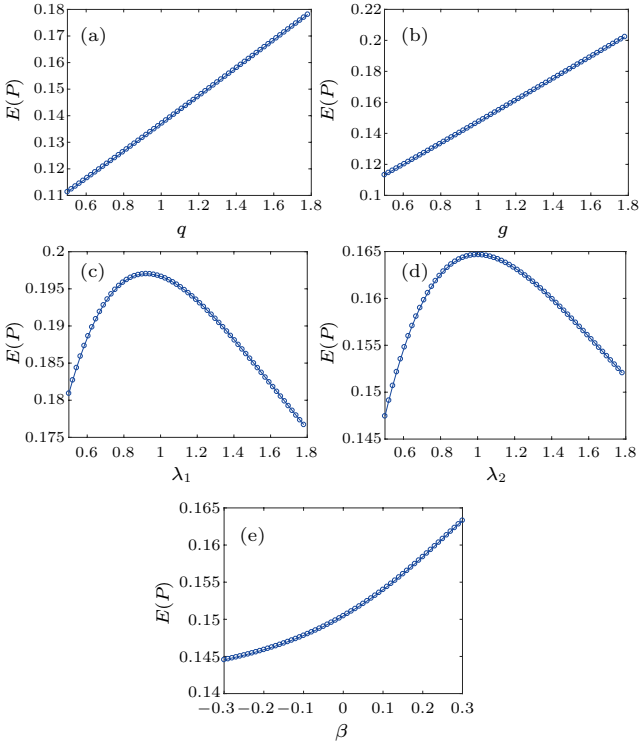


Fig. 9. Evolution of $E(P)$ versus q, g, λ_1, λ_2, and β for fixed $\gamma = 0.8$, with (a)–(e) $\sigma = 1$.

Figure 9 shows the effects of the parameters q, g, λ_1, λ_2, and β on the mean output power $E(P)$. $E(P)$ increases with the increase of q, g or β as shown in Figs. 9(a), 9(b), and 9(e), which reveal that system performance can be improved by increasing these parameters. However, $E(P)$ firstly heightens and then reduces with the increase of λ_1 or λ_2 in Figs. 9(c) and 9(d). This indicates that there exist optimal $\lambda_1 = 0.941$ and $\lambda_2 = 1.004$ that maximize the mean output power $E(P)$ for fixed $\varepsilon = 0.1$, $\beta = 3$, $\omega = 1.5$, $F = 1.6$, $\beta_1 = 1$, $\mu = 2$, $q = 1.2$, $g = 1$, $\lambda_1 = 3$, $\lambda_2 = 2$, $\sigma = 1$, and $\gamma = 0.8$, which can contribute to improvement of the energy harvesting performance.

Figures 10(a) and 10(b) depict $E(a^2)$ and $E(P)$ increasing with β or γ. This suggests that a larger viscoelastic parameter or random excitation can improve the power output.

Figure 11 presents comparisons of $E(P)$ among the piezoelectric VEH, electromagnetic VEH, and hybrid VEH. It can be seen that $E(P)$ of the piezoelectric or electromagnetic VEH is lower than that of the hybrid VEH. This reveals that the hybrid EHS is more efficient at harvesting energy than the piezoelectric or electromagnetic EHS.

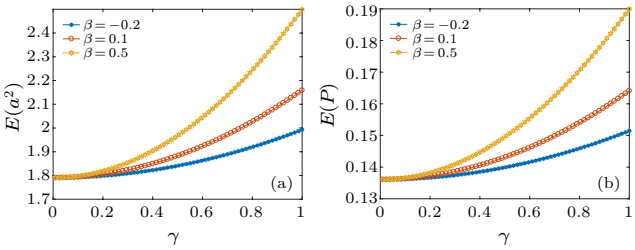


Fig. 10. (a) $E(a^2)$ and (b) $E(P)$ versus random excitation γ under different viscoelastic parameters β for $\sigma = 1$.

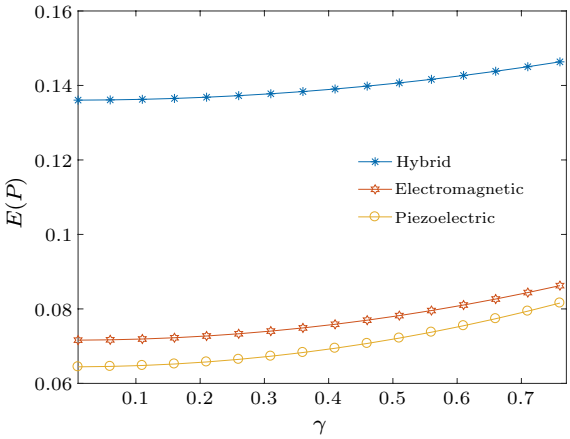


Fig. 11. Comparisons of $E(P)$ among hybrid harvester, electromagnetic harvester, and piezoelectric harvester ($\sigma = 1$).

5. Conclusions

In summary, we have investigated the stochastic responses of the hybrid vibration EHS with a viscoelastic material under narrow-band noise, and revealed the influence of system parameters on $E(v^2)$, $E(i^2)$, and $E(P)$.

The model of the hybrid VEH is briefly introduced, including the dimensionless system governing the equations derived by variable substitutions. Employing the multi-scales method, we obtain the first-order approximate solutions for the hybrid vibration EHS, and then derived the steady-state amplitude-frequency response formula and the FSSM for the amplitude. The numerical solutions obtained utilizing the Monte Carlo method are provided to verify the effectiveness of the method. The results show a good agreement between the numerical and approximate analytical solutions. Lastly, the effects of parameters q, g, γ, β, λ_1, and λ_2 on $E(v^2)$, $E(i^2)$, and $E(P)$ are discussed.

The main conclusions are provided as follows: (1) Enlarging the electromechanical coupling coefficients q and g makes $E(v^2)$ and $E(i^2)$ decrease but makes $E(P)$ increase almost linearly. It is illustrated that increasing the electromechanical coupling coefficients can increase the efficiency of the hybrid EHS. (2) $E(v^2)$ and $E(i^2)$ increase with increasing λ_1 and λ_2, but $E(P)$ firstly increases and then decreases with increasing λ_1 and λ_2, meaning that the optimal values of λ_1 and λ_2 can be obtained to maximize the efficiency of energy harvesting. (3) $E(v^2)$, $E(i^2)$, and $E(P)$ increase with the increases of the viscoelastic parameter β and the random excitation γ, suggesting that the increases of β and γ are beneficial to improving the efficiency of the hybrid EHS.

By comparing the piezoelectric EHS, electromagnetic EHS and hybrid EHS, it is found that the hybrid EHS has better energy harvesting efficiency than either the single electromagnetic EHS or the single piezoelectric EHS.

Acknowledgments

This work is supported by the National Natural Science Foundation of China (Grant Nos. 12002089 and 11902081), the Science and Technology Projects in Guangzhou (Grant Nos. 202201010326 and 2023A04J1323), and the Guangdong Basic and Applied Basic Research Foundation (Grant No. 2023A1515010833).

References

[1] Tuoi T T K, Toan N V and Ono T 2022 *Appl. Energy* **311** 118679
[2] Prajwal K T, Manickavasagam K and Suresh R 2022 *Eur. Phys. J. Special Top.* **231** 1359
[3] Jiang C M, Li X J, Lian S W M, Ying Y, Ho J S and Ping J F 2021 *ACS Nano* **15** 9328
[4] Ren Z W, Wu L T, Pang Y K, Zhang W Q and Yang R S 2022 *Nano Energy* **100** 107522
[5] Manthiram A 2009 *Energy Harvesting Technologies: Materials for High-energy Density Batteries* (New York: Springer) pp. 365–385
[6] Roundy S and Wright P K 2004 *Smart Mater. Struct.* **13** 1131
[7] Ooi B L and Gilbert J M 2014 *Sens. Actuators A* **213** 9
[8] Karami A, Basset P and Galayko D 2015 *J. Phys.: Conf. Ser.* **660** 012025
[9] Ibrahim A, Ramini A and Towfighian S 2020 *Energy Rep.* **6** 2490
[10] Challa V R, Prasad M G and Fisher F T 2009 *Smart Mater. Struct.* **18** 095029
[11] Karami M A and Inman D J 2011 *J. Sound Vib.* **330** 5583
[12] Li P, Gao S Q and Cai H T 2015 *Microsyst. Technol.* **21** 401
[13] Mokem F I S, Nono D B C, Siewe S M and Tchawoua C 2018 *Commun. Nonlinear Sci. Numer. Simul.* **56** 177
[14] Fan K Q, Tan Q X, Liu H Y, Zhu Y M, Wang W D and Zhang D X 2018 *Smart Mater. Struct.* **27** 085001
[15] Sun Y H, Yang Y G, Zhang Y and Xu W 2021 *Chaos* **31** 013111
[16] Rong H W, Xu W and Fang T 1998 *J. Sound Vib.* **210** 483
[17] Liu D, Xu Y and Li J L 2017 *Chaos Solitons Fractals* **104** 806
[18] Jin Y F and Zhang Y X 2021 *Acta Mech.* **232** 1045
[19] Huang Z L and Jin X L 2009 *J. Sound Vib.* **319** 1121
[20] Xiao S M and Jin Y F 2017 *Nonlinear Dyn.* **90** 2069
[21] Zhang Y X, Jin Y F and Xu P F 2020 *Int. J. Mech. Sci.* **172** 105418
[22] Zhu H T and Guo S S 2015 *J. Vib. Acoust.* **137** 041015
[23] Shi T T, Xu X M, Sun K H, Ding Y P and Huang G W 2020 *Chin. Phys. B* **29** 050501
[24] Lin B W, Wang Y H and Qian Y H 2022 *Eur. Phys. J. Plus* **137** 459
[25] Su M, Xu W and Zhang Y 2021 *Eur. Phys. J. Plus* **136** 271
[26] Jiang W A, Ma X D, Han X J, Chen L Q and Bi Q S 2020 *Chin. Phys. B* **29** 100503
[27] Burstein A H and Frankel V H 1968 *Ann. New York Acad. Sci.* **146** 158
[28] Zhou X Q, Yu D Y, Shao X Y, Zhang S Q and Wang S 2016 *Compos. Struct.* **136** 460
[29] Fan R P, Meng G, Yang J and He C C 2009 *J. Sound Vib.* **319** 58
[30] Cortés F and Elejabarrieta M J 2007 *Mater. Design* **28** 2054
[31] Gröhlich M, Lang A, Bswald M and Meier J 2021 *Mater. Design* **207** 109885
[32] Xu Y, Li Y G and Liu D 2014 *J. Comput. Nonlinear Dyn.* **9** 031015
[33] Guo S L, Yang Y G and Sun Y H 2021 *Chaos Solitons Fractals* **151** 111231
[34] Wu S T 2011 *Acta Math. Sci.* **31** 1436
[35] Xu W, Rong H W and Fang T 2003 *Appl. Math. Mech.* **24** 61
[36] Floris C 2011 *Mech. Res. Commun.* **38** 57
[37] Denoël V 2018 *Probab. Engin. Mech.* **53** 66
[38] Yang Y G, Huang M L, Guo S L and Sun Y H 2023 *Mech. Syst. Signal Process.* **186** 109837
[39] Yang Y G, Guo S L and Sun Y H 2022 *Eur. Phys. J. Plus* **137** 1091
[40] Yang Y G, He L L, Zeng Y H, Sun Y H and Xu W 2022 *Int. J. Nonlinear Mech.* **147** 104230
[41] Zeng Y H, Yang Y G, Sun Y H and Zhang Y 2022 *Machines* **10** 1108
[42] Erturk A and Inman D J 2011 *Piezoelectric Energy Harvesting: Modeling and Exploiting Mechanical Nonlinearities in Piezoelectric Energy Harvesting* (New York: John Wiley and Sons) pp. 233–271
[43] Sarker M R, Julai S, Sabri M F M, Said S M, Islam M M and Tahir M 2019 *Sens. Actuators A* **300** 111634
[44] Iqbal M, Malik M N, Khan F, Abas P E, Cheok Q, Iqbal A and Aissa B 2020 *Int. J. Energy Res.* **45** 1
[45] Karami M A and Inman D J 2011 *J. Sound Vib.* **330** 5583
[46] Tran N, Ghayesh M H and Arjomandi M 2018 *Int. J. Engin. Sci.* **127** 162
[47] Harne R L and Wang K W 2013 *Smart Mater. Struct.* **22** 023001
[48] Zhao X R, Xu W, Gu X D and Yang Y G 2015 *Physica A* **431** 128
[49] Liu Q, Xu Y and Kurths J 2020 *Commun. Nonlinear Sci. Numer. Simul.* **84** 105184
[50] Li D X, Xu W, Yue X L and Lei Y M 2012 *Nonlinear Dyn.* **70** 2237
[51] Wedig W V 1990 *Struct. Safety* **8** 13
[52] Holmes M H 2013 *Introduction to Perturbation Methods: Multiple Scales* (New York: Springer) pp. 139–221
[53] Han Q, Xu W and Sun J Q 2016 *Physica A* **458** 115